Title
Lepidocrocite Titanate–Graphene Composites for Sodium-Ion Batteries

Journal
The Journal of Physical Chemistry C, 126(45)

ISSN
1932-7447

Authors
Barim, Gözde
Yin, Wei
Lin, Jason
et al.

Publication Date
2022-11-17

DOI
10.1021/acs.jpcc.2c06180

Lepidocrocite Titanate - Graphene Composites for Sodium-Ion Batteries

Gözde Barim[1], Wei Yin[1], Jason Lin[1], Chengyu Song[2], Tevye R. Kuykendall[3], Kenneth J. Takeuchi[4,5,6,7], Esther S. Takeuchi[4,5,6,7], Amy C. Marschilok[4,5,6,7], Marca M. Doeff[1,*]

1. Energy Storage & Distributed Resources Division, Lawrence Berkeley National Laboratory, Berkeley, CA, 94720, USA.
2. National Center for Electron Microscopy, Molecular Foundry, Lawrence Berkeley National Laboratory, CA, 94720, USA.
3. Molecular Foundry, Lawrence Berkeley National Laboratory, CA, 94720, USA.
4. Department of Chemistry, Stony Brook University, Stony Brook, NY, 11794, USA.
5. Department of Materials Science and Chemical Engineering, Stony Brook University, Stony Brook, NY, 11794, USA.
6. Energy and Photon Sciences Directorate, Brookhaven National Laboratory, Upton, NY, 11973, USA.
7. Institute for Electrochemically Stored Energy, Stony Brook University, Stony Brook, NY 11794, USA.

E-mail: mmdoeff@lbl.gov

ABSTRACT

To overcome electronic transport issues of layered titanates in sodium-ion batteries, we have designed and synthesized composites of lepidocrocite titanates with reduced graphene oxide through a solution-based self-assembly approach. The parent lepidocrocite titanate ($K_{0.8}[Ti_{1.73}Li_{0.27}]O_4$) was exfoliated by a soft-chemical approach and mechanical shaking. Exfoliated layered titania sheets (LTO) were then combined with reduced graphene oxide (rGO) layers to assemble into composites through flocculation. Counter cations (*i.e.,* Mg^{2+}) were used for the self-assembly of negatively charged titania and rGO nanosheets via flocculation. The carbon content in the composites was tuned from 1 to 17% by changing the ratio of titania and rGO sheets in the mixed colloidal suspensions. Electrodes were processed with as-prepared LTO-rGO composites without any carbon additives and tested in sodium half-cell configurations. Mg^{+}-coagulated LTO-rGO composite electrodes deliver higher capacities than electrodes prepared with coagulated titania sheets and 10% acetylene black in sodium half-cells and display good capacity retention after 50 cycles. Electrochemical impedance spectroscopy results indicate lower charge transfer resistance for LTO-14.5%rGO composites than that of coagulated titania sheets with 10% acetylene black. A power law analysis of cells containing the composites indicate a hybrid mechanism consisting of both surface and diffusional processes. A comparison with a similar system, that of dopamine-derived LTO-C heterostructures, reveal significant differences. While capacities showed a strong dependence on carbon content for the dopamine-derived materials, this was not true for the LTO-rGO composites. Instead, the highest capacity was obtained for the 14.5% rGO sample, with a lower value obtained for the 17% rGO sample. A greater proportion of the redox processes were surface rather than diffusional in nature for the LTO-rGO composites as well.

Keywords: Sodium-ion batteries, lepidocrocite titanates, intercalation anodes, self-assembly, reduced graphene oxide

INTRODUCTION

Sodium ion batteries are a promising energy storage technology for large-scale grid storage applications where cost and resource constraints are main concerns. The energy density, power density, and longevity of sodium ion batteries are limited by the available anode materials. Promising alternatives for sodium ion battery negative electrodes are ternary alkali titanates, some of which have layered or tunnel structures that reversibly intercalate sodium ions at low potentials (~0.3 - 0.6 V *vs.* Na^+/Na).[1–5] Their low cost, high tap density and relatively higher operating voltage that may prevent metallic sodium plating, makes them safer and denser alternatives to hard carbon electrodes, which are widely used in sodium-ion batteries. Titanates are also attractive anode materials owing to their low cost, low toxicity, and high abundance. However, many titanate structures have a finite number of sites for ion insertion, which limits the Na^+ storage capacities, and thereby the achievable energy density. The poor electronic conductivity and sluggish Na^+ (de)insertion kinetics are other impediments to the practical capacity and rate capability. Hence, copious amounts of carbon additives are often employed to enhance electrical conductivity in the electrode composites.

There have been several reports of lepidocrocite titanates used as anodes in sodium systems.[6–8] These materials have corrugated layered structures and are typically synthesized directly with large cations (K, Rb, Cs) between the titania layers. The layers may contain a wide range of substituents or vacancies and titanium is always in the tetravalent state.[4,9–11] The as-made lepidocrocite potassium titanate ($K_{0.8}Ti_{1.73}Li_{0.27}O_4$, KTL) has a theoretical capacity of 180 mAh/g based on site considerations, but delivered only 25 mAh g^{-1} in a sodium half-cell configuration.[6] The sodium ion exchanged form, in contrast, could insert 140 mAh g^{-1}, indicating that the identity of the interlayer cation is critical for good electrochemical performance.[6] Recently, we utilized a similar ion-exchange strategy to overcome site limitations in another lepidocrocite-type titanate ($Cs_{0.74}Ti_{1.815}\square_{0.185}O_4$, CTO).[8] Cs cations residing between titania layers were ion-exchanged with sodium ions and a non-stoichiometric sodium-containing analog ($Na_{0.74}Ti_{1.815}\square_{0.185}O_4 \cdot 1.27H_2O$, NTO) was obtained showing a high capacity of over 220 mAh g^{-1} thanks in part to the vacancies presented in the metal oxide layers. After electrode engineering with appropriate electrolyte and binder, we previously demonstrated a reversible capacity of 213 mAh g^{-1} for the vacancy-containing sodium analog with an average sodium insertion voltage of 0.6 V *vs.* Na^+/Na at a current rate of 20 mA g^{-1}.[8]

An effective way to overcome the low electrical conductivity and slow ion transport of layered titanates is to manipulate the electrode structure. Heterostructures, assembled by stacking different layered materials (*e.g.*, transition metal oxides, layered double hydroxides, graphene or reduced graphene oxides) can potentially overcome charge and ion transport issues.[11–14] These 2-dimensional (2D) heterostructures are interesting materials with unique structural and physical properties that none of the unilamellar 2D materials have alone.[15,16] These unique properties of 2D heterostructures stem from the variations in their work function, density of states, and Fermi energy positions. Synergistic effects, interfacial interactions, physical and quantum properties of individual components result in new properties and behavior.[15–18] The 2D architectures of heterostructures provide split-shaped ion diffusion channels for the facile transport of ions such as lithium or sodium.[19–22]

Xiong et al., described synthesis of a Ti-deficient 2D unilamellar lepidocrocite-type titanium oxide nanosheet superlattice through self-assembly of titania monolayers with functionalized reduced

graphene oxide sheets.[23] Calcination of self-assembled monolayers leads to the formation of alternately restacked defective titania sheets and nitrogen-doped graphene monolayers in the heterostructures. An exceedingly high capacity of 490 mAh g^{-1} at 0.1 A g^{-1} with an ultralong cycle life of 10000 was attributed to new sites created for sodium ions owing to the highly defect-rich nature of exfoliated titania layers.[23] The superlattice structure also enables a lower diffusion barrier for sodium (de)insertion without any significant phase or structure change. Recently, we reported the design and synthesis of heterostructures of titania sheets with carbonized dopamine to mitigate electronic transport issues in lepidocrocite-type titanates. Positively charged dopamine molecules were used as the carbon precursor and intercalated between negatively charged exfoliated titania sheets derived from $K_{0.8}Ti_{1.73}Li_{0.27}O_4$ (KTL) through electrostatic interaction. Dopamine-intercalated titania sheets were then annealed under argon to form conductive carbon layers between titania sheets. The carbon content in the heterostructures was tuned from 17.5 to 30% by changing experimental parameters.[24] Electrodes that were prepared by using as-prepared heterostructures without extra carbon additives exhibited higher capacities, better capacity retention over 100 cycles, and lower impedance when compared to titania sheets in sodium half-cell configurations. Improved capacity and degree of capacity retention was observed as the carbon content increased in the heterostructures, due to reduced charge transfer resistance in the composite electrodes. Power law analysis of cyclic voltammetry data, ex situ XRD and Ti K-edge X-ray absorption spectroscopy on pristine and partially or fully sodiated electrodes indicated that the redox mechanism in these materials is a combination of diffusional (intercalation) and surface (pseudocapacitive) reactions.

Here, we expand our exploration of carbon-containing heterostructures by combining titania sheets (LTO) with a different type of carbon (reduced graphene oxide (rGO)) to overcome the low electrical conductivity of the parent lepidocrocite-type potassium titanate ($K_{0.8}Ti_{1.73}Li_{0.27}O_4$). LTO-rGO composites were prepared by self-assembly with counter cations (e.g., Mg^{2+}) and the carbon content in the composites was tuned from 1% to 17% by changing the LTO/rGO ratio. Chemical, structural, and electrochemical characterization of heterostructures was conducted, and electrodes were prepared with and without additional carbon for electrochemical tests. LTO-rGO composite electrodes without carbon additives show good cycling capacity and capacity retention over 50 cycles in sodium half-cell configurations. Power Law analysis on cyclic voltammetry results indicates that the sodium (de)insertion reaction is more surface limited in these composites compared to the ones prepared with dopamine.

METHODS

Materials: Titanium (IV) oxide, anatase (Sigma, 99.8%), potassium carbonate (Alfa Aesar, 99%), lithium carbonate (Alfa Aesar, 99%), tetramethylammonium hydroxide solution (Sigma, 25 wt% in H_2O), ammonium persulfate (Alfa Aesar, 98%), graphene oxide dispersion (Graphanea, 0.4 wt% in H_2O), ammonia solution (Sigma, 28 wt% in H_2O), hydrazine solution (Sigma, 35 wt% in H_2O), magnesium nitrate hexahydrate (Strem, 99%), sodium nitrate (Alfa Aesar, 99%), potassium nitrate (Merck, 99%), lithium nitrate (Sigma, 99%).

Caution: Tetramethylammonium hydroxide is extremely toxic. An appropriate personal protective equipment needs to be used when handling and avoid contact with skin.

Preparation of titania sheets: The parent material potassium titanate ($K_{0.8}Ti_{1.73}Li_{0.27}O_4$) was prepared via a solid-state reaction of a stoichiometric mixture of TiO_2, K_2CO_3 and Li_2CO_3 at 900 °C for 20 hours (5 °C/min).[25] A soft-chemical method modified from the previous literature was used to exfoliate the as-synthesized product.[26] $K_{0.8}Ti_{1.73}Li_{0.27}O_4$ was protonated by stirring in 0.5 M ammonium persulfate (APS) solution at 60 °C for 3 hours (the solid-to-solution ratio was 4 g/L) and the solution was refreshed twice (total of 6 hours reaction in APS). The protonated product $H_{1.07}Ti_{1.73}O_4 \cdot H_2O$ was collected by filtration,

washed with water, and air dried at 60 °C. The powder was further stirred in a tetramethylammonium hydroxide solution ($(CH_3)_4NOH$, TMAOH) for a week under ambient conditions to obtain monolayers. The concentration of TMAOH corresponded to a molar equivalence of exchangeable protons in the protonated product, and the solid-to-solution ratio was 4 g/L. The exfoliated dispersion was centrifuged at 7500 rpm for 10 min to remove any unexfoliated material.

Preparation of composites: The concentration of exfoliated titania sheets was adjusted to 1.0 mg/mL and sonicated for 3 hours. The concentration of the graphene oxide dispersion was adjusted to 0.25 mg/mL and sonicated for an hour. Graphene oxide was reduced by hydrazine based on the previous literature.[27] The required amount of ammonia solution and hydrazine solution were added into the graphene oxide dispersion and kept at 90 °C for an hour. The reduced graphene oxide (rGO) was sonicated for an hour to disperse the restacked sheets. The titania sheets and reduced graphene oxide dispersion were combined and sonicated for an hour. The mixture was coagulated with Mg^{2+} cations by dropwise addition of 30 mL of 0.1 M $Mg(NO_3)_2$ solution while stirring for 120 mL of dispersion (1.0 mg/ mL). The mixture was stirred overnight at RT. The product was centrifuged at 9000 rpm for 10 min and washed with water twice, then freeze-dried. Mg-coagulated LTO nanosheets were prepared using the same procedure in the absence of rGO. LTO-rGO composites with other coagulants were also prepared by a similar approach. 0.1 M aqueous nitrate solutions of various cations (e.g., Li^+, Na^+, K^+) were used for self-assembly with a solid-to-solution ratio of 4 g/L. The LTO/rGO ratio of 85:15 was kept constant for the mixed titania and reduced graphene oxide suspensions before the addition of the aqueous coagulant solutions unless otherwise noted. An LTO-rGO mixture was also prepared without using any coagulants. For this, an LTO-rGO mixture with a ratio of 85:15 was sonicated for an hour, centrifuged at 11000 rpm for 15 min and then freeze-dried. Freeze-dried LTO nanosheets without coagulants were prepared similarly in the absence of rGO.

Characterization: Powder XRD data were collected on a Bruker D2 Phaser diffractometer with a CuKα source (λ = 1.5406 Å) equipped with a LynxEye detector, between 5 and 90° (2θ) at a rate of 0.0001°/s and a step size of 0.022°. Thermogravimetric analysis (TGA) was carried out in air with a heating rate of 10 °C/minute on a TA Instruments Q5500 TGA-MS instrument. Scanning electron microscopy (SEM) images were captured on a Zeiss Gemini Ultra55 Field Emission Scanning Electron Microscope (FESEM) equipped with a Bruker X-Ray Energy Dispersive Spectrometer (X-Ray EDS) for mapping and elemental analysis. Transmission electron microscopy (TEM) imaging was performed via FEI F20 UT Tecnai microscope, operated at an electron acceleration voltage of 200kV with a spacial resolution of 0.12 nm. Samples were dispersed in methanol and dropped onto a lacey carbon grid.

The electrochemistry analyses were conducted in two-electrode 2032-coin cells containing metallic sodium as the counter electrode. Sodium disks were made by shaping dry sodium cubes (Sigma-Aldrich) into thin foils and cutting to size. Composite working electrodes were prepared by making a slurry of 90 wt% of active material, and 10 wt% carboxymethyl cellulose (CMC)/Styrene-Butadiene Rubber (SBR) in aqueous binder solution. No carbon was added to the slurries unless otherwise noted. The slurries were then cast onto carbon-coated aluminum foil. The electrodes were dried under vacuum at 120 °C for 12 h before being cut to size and weighed. The typical loadings and thicknesses were ~ 1.0 – 1.5 mg cm^{-2} and ~30 μm, respectively. The tap density of the powder was 0.202 g/mL. A solution of 0.5 M $NaBPh_4$ (sodium tetraphenylborate, Alfa Aesar) solution in diethylene glycol dimethyl ether (DEGDME) was used as the electrolyte for sodium cells. Galvanostatic cycling experiments, cyclic voltammetry, and electrochemical impedance spectroscopy experiments were carried out at room temperature using a BioLogic VMP3 potentiostat/galvanostat. The cyclic voltammograms were obtained

between 0.1−2.0 V with scan rates of 0.05-1.0 mV/s. The impedance spectra were recorded in the frequency range of 200 kHz to 1.4 mHz at a 10 mV amplitude, after cells were discharged to 0.1 V or charged to 2.0 V using a current density of 0.15 mA cm^{-2}. Cells were rested for half an hour after the galvanostatic experiments before impedance data were collected.

The electrodes for X-ray absorption spectroscopy (XAS) measurements were cycled to specific states-of-charge, disassembled in an argon-filled glovebox, and subsequently washed with dimethyl carbonate to remove salt residue. The dried and washed electrodes were sealed with polyimide tape in an argon-filled glovebox and placed in aluminum pouches for transfer. All XAS measurements were carried out in both transmission and fluorescence modes at beamline 4-3 at SSRL. Calibration was applied to all spectra using the first inflection point of the reference Ti metal foil. XAS data were analyzed using Athena software.

RESULTS AND DISCUSSION

We used a two-step soft-chemical approach to exfoliate the parent lepidocrocite titanate (KTL, $K_{0.8}Ti_{1.73}Li_{0.27}O_4$). In the protonation step, we used ammonium persulfate (APS) solution to replace potassium and lithium cations between and within titania layers by hydronium ions. A swollen protonated structure was confirmed by powder XRD experiments. A shift in the position of the first peak from 2θ = 11.38° to 9.67° indicates expansion of layers from 0.78 to 0.97 nm after protonation (**Figure S1**). The protonated material was then exfoliated in tetramethylammonium hydroxide via mechanical shaking for a week. XRD patterns of the freeze-dried titania sheets exhibited a further shift of the low angle peak to 2θ = 7.99° corresponding to an interlayer spacing of 1.11 nm. Suspensions of exfoliated titania sheets exhibit good colloidal stability and dispersibility for several months without phase separation.

We prepared mixed titania and reduced graphene oxide suspensions with various LTO/rGO ratios to synthesize lepidocrocite titanate-reduced graphene oxide composites by self-assembly. The graphene oxide dispersion was first chemically reduced by hydrazine at 90 ℃ as previously described in the literature.[27] Negatively charged titania and reduced graphene oxide sheets in the mixed colloidal suspensions were self-assembled into composites by overnight mixing with an aqueous $Mg(NO_3)_2$ counter-cation solution. Coagulation of LTO and rGO sheets was observed immediately after the addition of the aqueous $Mg(NO_3)_2$ solution, leading to the flocculation of LTO-rGO composites in the suspension, and a homogenous black powder of the product was isolated after the self-assembly (**Figure S2**). Coagulation with aqueous $NaNO_3$ solution as comparison results in an inhomogeneous mixture which will be discussed in more detail later.

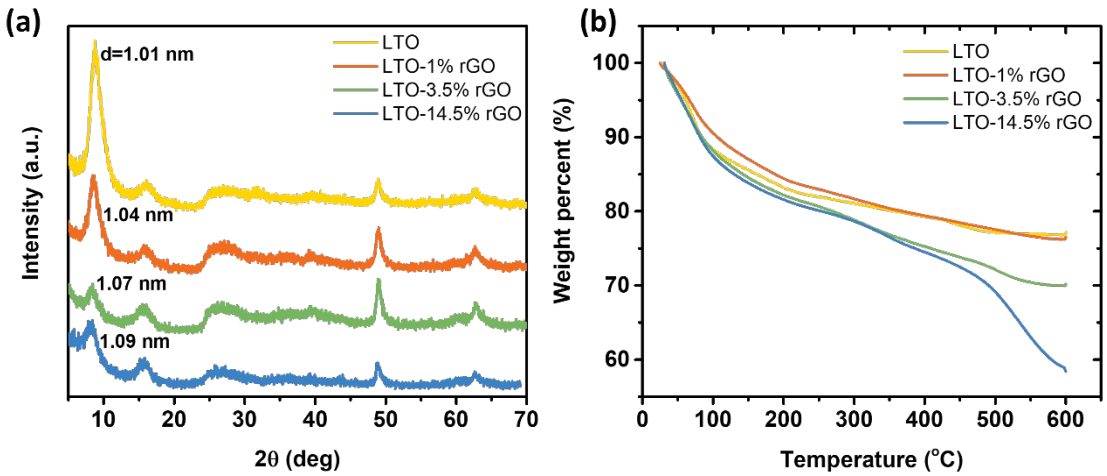

Figure 1: **(a)** XRD patterns and **(b)** TGA weight loss curves of lepidocrocite titanate – reduced graphene oxide composites coagulated by Mg^{2+} using various LTO/rGO ratios. The LTO sample was coagulated with Mg^{2+} and was rGO-free.

Figure 1a shows XRD patterns of as-prepared lepidocrocite titanate – reduced graphene oxide composites with various LTO/rGO ratios, along with Mg-coagulated titania sheets without rGO for comparison (LTO). The first broad peak was observed at 2θ = 8.77° for Mg-coagulated titania sheets which corresponds to an interlayer spacing of ~1.01 nm. (**Figure 1a**). A shift to 8.6° for the LTO-1%rGO composite indicates an increase in the interlayer spacing to ~1.04 nm. As the reduced graphene oxide content was further increased to 3.5 and 14.5% in the LTO-rGO composites, a shift in the first peak position towards lower angles was further realized indicating expansion of interlayer spacing to ~1.07 and ~1.09 nm, respectively (**Figure 1a**). TGA was used to determine carbon and water content in the LTO-rGO composites. The weight loss up to 350 °C is associated with loss of water in the composites, with that below 100 °C due to the evaporation of physiosorbed water, and that between 100°C to 350°C corresponding to the removal of structural (interlayer) water. The loss in weight between 350 and 600 °C is associated with the removal of carbon from the composites. A 20% reduction in the weight for Mg-coagulated titania sheets in the absence of rGO stems from the removal of physiosorbed and structural water (**Figure 1b**).

Figure S3 shows the correlations between interlayer spacing and water and/or carbon content determined by the weight loss in the TGA experiments of the LTO-rGO composites prepared with various LTO/rGO ratios. The interlayer spacing increases in a linear fashion with carbon content roughly obeying Vegard's Law (**Figure S3a**), but there is a better fit when both carbon and water content are taken in account (**Figure S3c**). Weight loss associated with the water removal is relatively invariant at approximately 20% for all Mg-coagulated LTO-rGO composites and about half of it is due to evaporation of physiosorbed water. Roughly 10% of the water is structural with no clear relationship to physical characteristics such as carbon content, similar to the water content of Mg-coagulated titania sheets in the absence of rGO (**Figure S3b,d**). LTO-1%rGO and LTO-17%rGO samples were dried in Argon at 160°C for 12h. A 0.4 and 0.6 Å decrease in the interlayer spacing was observed for these, respectively, after drying, indicating loss of structural water (**Figure S4**). Although, there is no correlation of water content

with carbon content, there is an obvious linear relationship between the sum of carbon content and water content and d-spacing (**Figure S3c**). These results strongly suggest that carbon and roughly half of the water is located in interlayer spaces.

Figure 2 displays TEM micrographs of LTO-8.5%rGO composites at low and high magnifications. The low magnification TEM image indicates that this material has a sheet-like morphology (**Figure 2a**). Three different interlayer spacings of ~ 0.35, 0.8 and 1.1 nm were found in various particles and different parts of the same particle. The 1.1 nm spacing is attributed to alternating layers of titania and graphene sheets, which agrees well with the XRD results. The 0.35 nm and 0.8 nm interlayer spacings might be associated with restacked reduced graphene oxide and titania layers, respectively, suggesting inhomogeneities in the coagulated samples or polycrystalline nature of the composites.

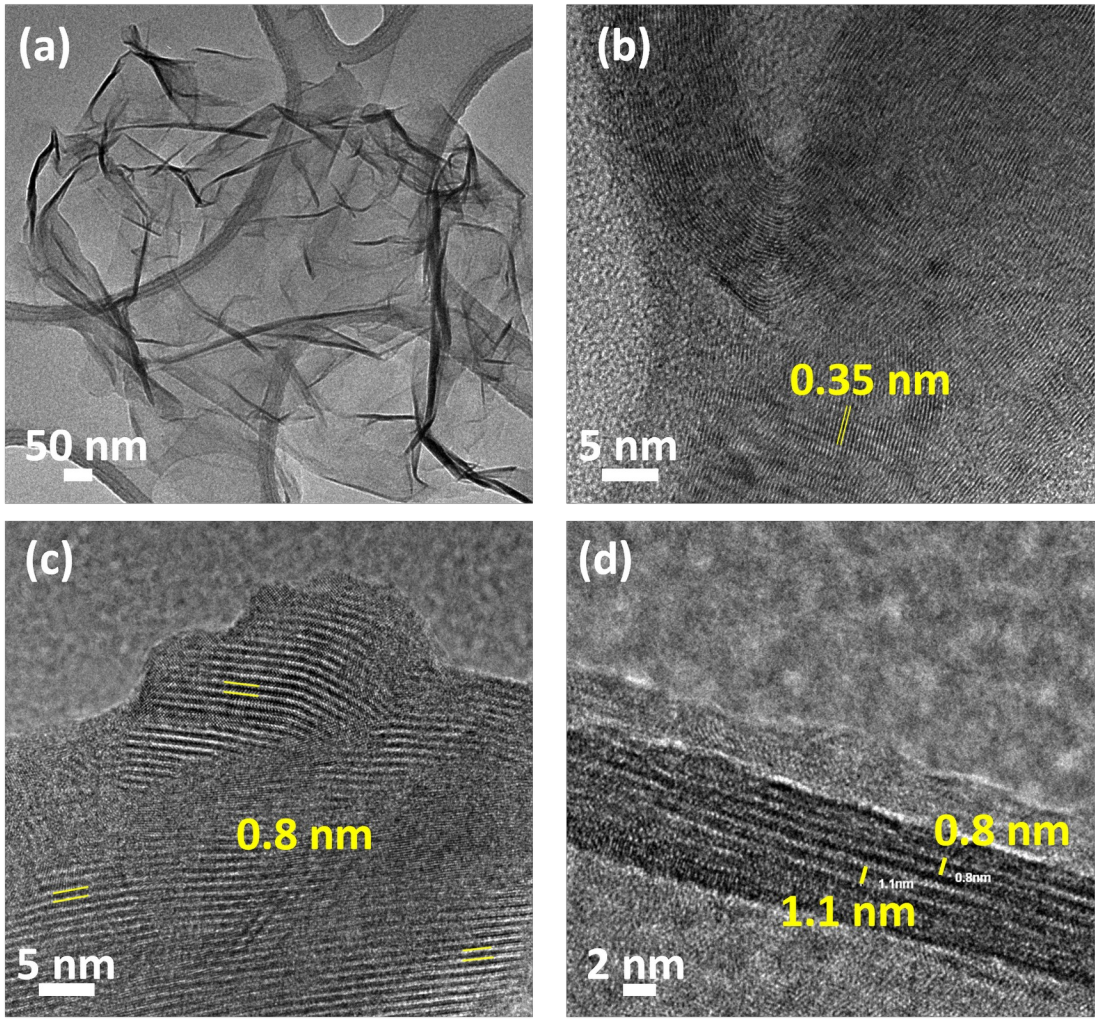

Figure 2: **(a)** TEM, **(b)**, **(c)** and **(d)** HRTEM micrographs LTO-8.5%rGO composites. Repeating layer spacings of ~0.35, 0.8 and 1.1 nm were indicated with yellow lines.

We also used other counter-cations (i.e., Li^+, Na^+, K^+) to coagulate titania and reduced graphene oxide sheets. **Figure S5** shows the XRD patterns of the as-prepared lepidocrocite titanate – reduced graphene oxide composites coagulated with different counter-cations. A significantly lower interlayer spacing of ~ 0.87 nm was observed for the LTO-rGO composites prepared with monovalent Li, Na and K cations compared to that of Mg^{2+} coagulated composites under otherwise identical conditions. This discrepancy in the interlayer spacing is most likely attributable to the higher hydration of the magnesium cation. The divalent Mg^{2+} has the smallest ionic size and highest charge density compared to the monovalent cations used in this study. This increase in the charge density leads to more hydration in the case of Mg^{2+} and more water is incorporated into the structures during coagulation.[28,29] The physical properties of these samples are summarized in **Table S1**. Powders of the composites also exhibit heterogeneity, suggesting random self-assembly between titania sheets and reduced graphene oxide layers rather than interleaved structures (**Figure S2**). Even after doubling the concentration of the aqueous $NaNO_3$ solution, similar results were obtained, suggesting that the distinction between the results do not solely stem from the difference in the charge on the counter-cations (**Figure S6**). **Figure S7** shows SEM micrographs of LTO-rGO composites prepared with various counter-cations, along with the freeze dried LTO-rGO mixture without coagulants, as well as the Mg-coagulated titania sheets in the absence of rGO. A uniform morphology was observed in the case of the Mg-coagulated LTO-rGO composites and titania nanosheets (**Figure S7a,c**). However, Li, Na and K coagulated LTO-rGO composites exhibit differences in the contrast of particles. Brighter particles correspond to titania sheets whereas the darker ones indicate reduced graphene oxide. A similar morphology and phase segregation were observed in the case of the freeze dried mixed LTO-rGO suspension in the absence of counter-cations. The morphologies of Mg-coagulated LTO-rGO composites with a broad range of carbon content from 1% to 14.5% were also characterized by scanning electron microscopy. SEM micrographs show that these samples have a homogenous porous sheet-like morphology without any obvious contrast in particles (**Figure S8**). **Figure S9** shows SEM micrographs of LTO-14.5%rGO composites along with elemental mapping. Homogenous distributions of Ti, O and Mg were observed, but slightly higher C distributions are detected on some parts of the particles. The 18% carbon quantified by EDX analysis is slightly higher than the TGA analysis, which also suggest variation of carbon content in the particles.

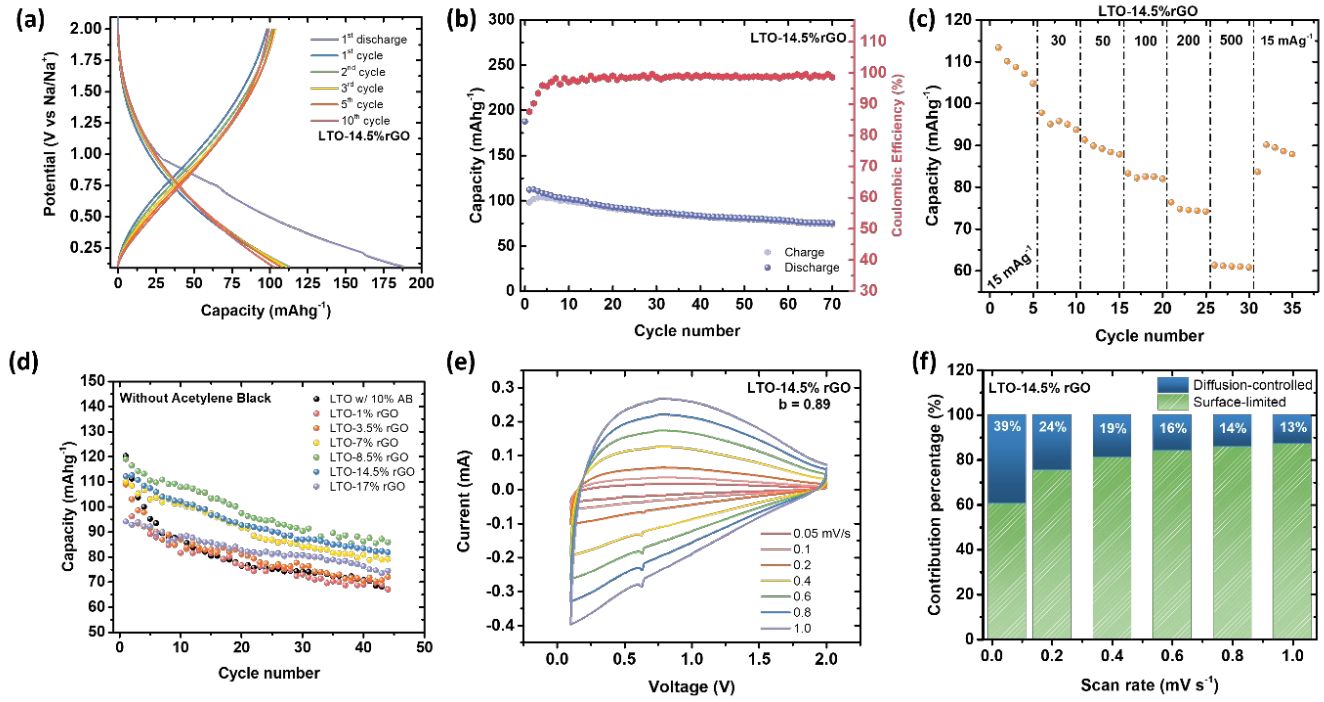

Figure 3: **(a)** Voltage profile of sodium half-cells containing LTO-14.5% rGO electrodes during the first few cycles **(b)** cycling performance at 15 mA g^{-1} (0.15 mA cm^{-2}) for 70 cycles and **(c)** rate performance of cell containing the LTO-14.5%rGO composite. **(d)** Cycling performance of cells containing LTO-rGO composites with various carbon contents at 15 mA g^{-1} for 45 cycles. (Na-insertion (discharge) capacities are displayed.) **(e)** Cyclic voltammograms of a cell containing the LTO-14.5%rGO composite at different scan rates from 0.05 to 1.0 mV/s, and **(f)** normalized contributions of diffusion-controlled and surface-limited reactions at different scan rates. No additional carbon was used in the LTO-rGO composite electrodes, but the LTO electrode contained 10% acetylene black.

We assessed the electrochemistry of LTO-rGO composites with various rGO contents in 2032-type coin cells in sodium half-cell configurations. Composite electrodes were prepared with as-synthesized active materials and 5 wt% carboxymethyl cellulose (CMC)/5 wt% Styrene-Butadiene Rubber (SBR) binder without any additional carbon. **Figure 3a** shows the first few charge and discharge profiles of the LTO-14.5%rGO composite at a current density of 15 mA g^{-1} between 0.1V and 2.0V. The voltage profile is sloping and featureless. An initial discharge capacity of 187 mAh g^{-1} was obtained, of which 98 mAh g^{-1} was recovered in the first charge. The first cycle Coulombic efficiency was determined to be 52% and an increase in the Coulombic efficiency to 99% was observed after ten cycles. On subsequent cycles, the Coulombic efficiency remained around 99%, and the cell retained 67% of its second discharge capacity after 70 cycles (**Figure 3b**). This result suggests good structural stability. The loss in the first cycle is due to formation of a solid-electrolyte interphase, decomposition of binder, decomposition of adventitious water, and side reactions between electrolyte and binder at low potentials. An average operating potential of 0.6 V *vs.* Na^+/Na was measured, comparable to the previous reports on the lepidocrocite type sodium titanates, and lower than that of anatase TiO_2 (0.8 V *vs.* Na^+/Na).[6–8,24,30] Rate capability results using current densities ranging from 15 to 500 mA g^{-1} are presented in **Figure 3c**. While

capacities decreased as the current was raised, the starting capacity was partially recovered after reversing the current density to 15 mA g^{-1}. The electrochemistry of LTO-rGO composites with various carbon contents were also evaluated in sodium half-cell configurations. Second discharge capacities generally trended modestly higher as the rGO content in the composites increased (**Figure 3d**) with the exception of the one containing 17.5%, which showed similar performance to cells containing the composites with low rGO content. A cell containing an electrode made with freeze-dried titania nanosheets without rGO and Mg^{2+}-coagulant with 10% acetylene black showed almost no electrochemical activity (**Figure S10b**), while one with Mg^{2+}-coagulated titania sheets performed much better. The cell labeled LTO in **Figure 3d** contained an Mg^{2+}-coagulated titania nanosheet electrode to which 10% acetylene black has been added. This had a lower capacity and lower first cycle Coulombic efficiency of 50% compared to almost all of those containing the LTO-rGO composites with the exception of the one with only 1% rGO. In addition, the capacity retention was poorer. **Figure S11** shows electrochemical cycling of cells containing LTO-rGO composite electrodes prepared with 20% acetylene black as well as the voltage profile of acetylene black powder alone during the first five cycles. There is about a 20 mAh g^{-1} increase in the discharge capacities for all LTO-rGO composites, which can be ascribed to the contribution from acetylene black (**Figure S11b**). Acetylene black powder by itself delivers a reversible capacity of about 70 mAh g^{-1} in sodium-half cells (**Figure S11c**). Electrodes consisting of rGO powder alone, processed similarly to the titania heterostructures, were electrochemically inactive in sodium half-cell configurations.

Cyclic voltammetry was carried out at different scan rates to gain further insight into the sodium insertion mechanism into the LTO-14.5%rGO composite. The CV curves demonstrate a small peak around 0.62 V, and a quasi-rectangular shape suggesting a partially pseudocapacitive sodium insertion mechanism (**Figure 3e**). We performed kinetic analysis on the CV curves at various scan rates to evaluate the mechanism of sodium storage. The b value can be obtained from the relationship between peak current (i) and scan rate (ν): $i = a\nu^{b}$, where a value of 0.5 indicates diffusion-controlled insertion and 1.0 a surface-limited capacitive mechanism. A b value of 0.89 was estimated by plotting $\log(\nu)$ versus $\log(i)$, suggesting a hybrid process involving both a slow diffusion-controlled process and a fast capacitive-like mechanism. We observed a similar hybrid process for a cell with a vacancy-containing lepidocrocite titanate ($Na_{0.74}Ti_{1.815}\square_{0.185}O_4 \cdot_{1.27}H_2O$), which exhibited two distinct peaks at low and high potentials with b values of 0.67 and 0.78, respectively. An increase in the b value to 0.92 in the high voltage region was observed after air exposure suggesting high hygroscopicity and the increase in the surface-controlled absorption was attributed to formation of extra redox active sites on the surface by reaction with water.[8] The contributions of the surface-limited capacitive and diffusion-controlled mechanisms were determined by separating the peak current (i) at a fixed voltage: $i = k_1\nu + k_2\nu^{1/2}$. The contribution of the diffusion-controlled intercalation process was determined to be 39% at a scan rate of 0.05 mV s^{-1} indicating the importance of the surface-controlled kinetics even at slow scan rates (**Figure 3f**). This gradually decreased to 13% as the scan rate was raised to 1.0 mV s^{-1}. **Figure S12** compares results for cells with the LTO-3.5% rGO, LTO-14.5% rGO, and LTO nanosheet electrodes containing acetylene black. The LTO nanosheet electrode with 20% acetylene black exhibit less diffusion-controlled behavior than the LTO-rGO electrodes with a contribution percentage of 26% (**Figure S12**). The shape of the CV is also different, with several quasi-reversible peaks exhibited. For the LTO-rGO electrodes, an increase in the b value from 0.86 to 0.89 as the rGO amount increased from 3.5% to 14.5% indicates that the capacitive behavior is weakly linked to carbon content. The contribution of the diffusion-controlled mechanism at 0.05 mVs^{-1} also decreased from 47 to 39% when the rGO content decreased. We reported a similar hybrid capacitive/intercalation behavior for dopamine-derived LTO-30%C heterostructures. However, the

contribution of the diffusion-controlled mechanism (75%) was much higher at a 0.05 mVs^{-1} scan rate for this material.[24] We speculate that Mg in the LTO-rGO composites may block or inhibit diffusion of sodium, resulting in a lower overall capacity for these materials compared to those made with dopamine. The capacity as a function of carbon content also exhibits different behavior in LTO-rGO system. In the dopamine system, capacity increases with the carbon content. For LTO-rGO, the capacity drops off at 17% carbon. However, the range of carbon content (from 17.5 to 30%) was higher for the dopamine system. This suggests that the carbon in the dopamine system may contribute more capacity than the rGO does. The complex structure of the LTO-rGO composites, which consist of interleaved LTO and rGO, as well as areas of restacked LTO and rGO, complicate interpretation of the electrochemical results. It is, however, likely, that a high rGO content is deleterious to the electrochemical capacity if it increases the content of restacked rGO in the sample, given its electrochemical inertness.

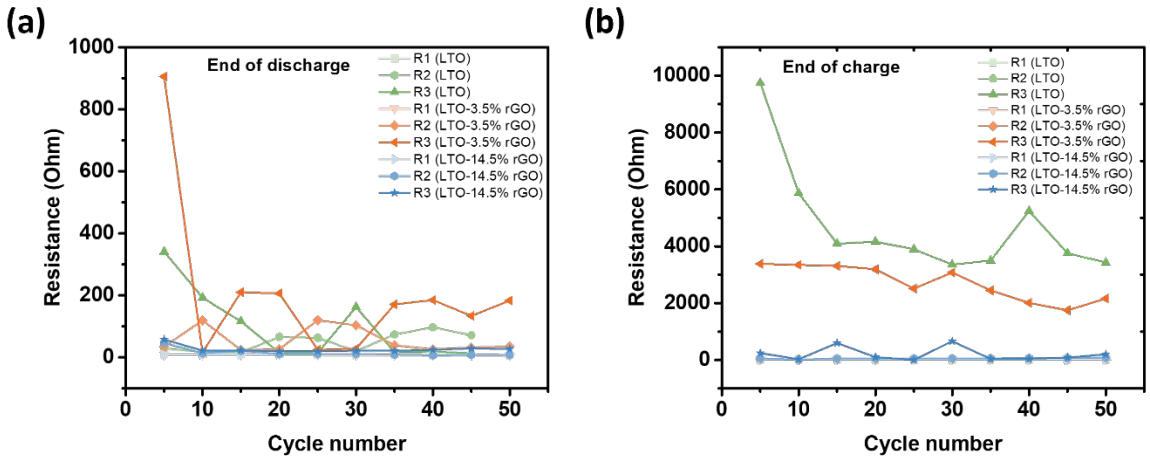

Figure 4: R1, R2, and R3 values of Na/LTO-rGO and Na/LTO cells extracted from Nyquist plots after the end of the selected **(a)** discharge and **(b)** charge cycles. LTO-rGO electrodes contained either 3.5% or 14.5% rGO but no added carbon, while LTO electrodes contained 10% acetylene black. Cells were rested for half an hour before impedance data was collected.

Electrochemical impedance spectra (EIS) were obtained to evaluate the resistance of sodium half-cells containing electrodes with LTO-3.5%rGO, LTO-14.5% rGO or Mg-coagulated LTO nanosheets. The latter electrodes contained 10% acetylene black, whereas no carbon was added to the electrodes containing the composites. **Figure S13** shows Nyquist plots of the cells, which consist of two semi-circles at high and middle frequencies and a straight line at low frequencies. The intercept of the high frequency semicircle with the real axis (R1) is the Ohmic resistance of all the cell components. This semicircle contains information about processes at the sodium electrode (R2, charge transfer resistance, solid electrolyte interphase, etc.). The second semicircle at middle frequencies is associated with processes at the composite electrode (R3), and the straight line at low frequencies is due to the ionic diffusion (Warburg diffusion) in the electrode. These assignments are based on analogies to similar cells.[1,24] The interfacial impedance of sodium anodes can vary considerably depending on electrolyte and usage.[31] In general, these values tend to be low when glymes are used as solvents in electrolytic solutions, although they vary somewhat with the type of salt used.[32] A system nearly identical to the one presented

here shows comparably low values for the interfacial resistance at the sodium electrode.[33] Thus, we feel confident that the high frequency semi-circle can be assigned to this phenomenon.

Comparable R1 values, which did not vary with cycle number, were observed after selected charge and discharge cycles, indicating similar Ohmic resistances of cell components for all the cells (**Figure 4**). R2 values at the end of selected discharge cycles are significantly lower for the Na/LTO-14.5%rGO cell compared with those of Na/LTO-3.5%rGO and Na/LTO-10%AB and display somewhat random variation in a narrow range with cycling. However, the biggest contribution to overall cell impedance is R3 for the LTO and LTO-3.5%rGO cells and they do not increase upon cycling. In contrast, the R3 values of Na/LTO-14.5%rGO cell are low and remain nearly constant throughout the charge and discharge cycles (**Figure 4a,b**) suggesting lower charge-transfer resistance for the former. The total impedance after the 15th discharge is lower than that of 1st discharge indicating good stability (**Figure S13**).

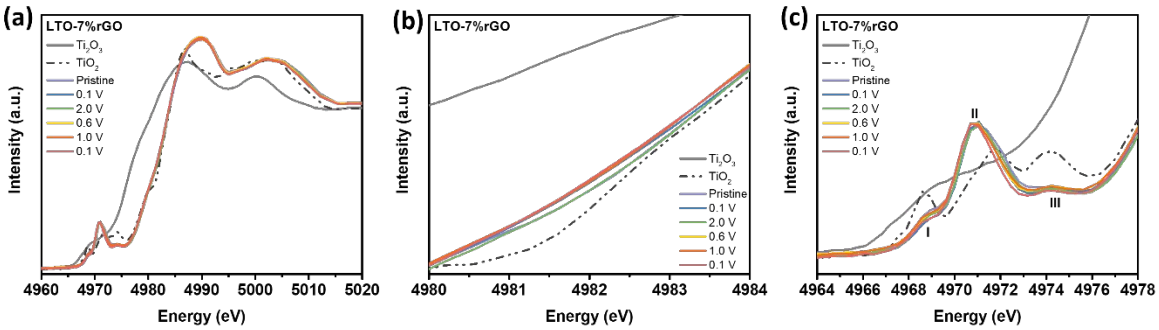

Figure 5: Ex situ Ti K-edge XAS measurements of LTO-7%rGO electrodes at various states-of-charge **(a)** whole spectra, **(b)** edge region and **(c)** pre-edge region. Electrodes were cycled at a current density of 15 mA g^{-1} to the indicated potentials. XAS spectra of Ti_2O_3 and TiO_2 are also included as references.

Ti K-edge synchrotron XAS was conducted to gain insight on the redox properties of the LTO-7%rGO composite electrode. This experiment gives information about bulk changes in the chemical environment and the electronic structure of the transition metal. The Ti K-edge position of pristine LTO-7%rGO appears at 4976 eV, very close to that found for TiO_2 and indicative of a +4 oxidation state (**Figure 5**). The edge positions of discharged and cycled electrodes shift to slightly lower energies suggesting minor reduction of Ti upon sodium insertion. However, the edge positions of the discharged electrodes are still much closer to the value found for TiO_2 than that of Ti_2O_3 implying that Ti has not been significantly reduced to Ti^{3+} (**Figure 5b**). The pre-edge region of XANES spectra yields information on metal coordination and chemical environment. Ti pre-edge region consists of three peaks labelled I-II-III that are associated with the transition of s1 core electrons of Ti to the unoccupied hybridized states of Ti 3d–4s/4p (**Figure 5c**). The peak I and peak II are related to the t_{2g} bonding states and the nondirectional e_g antibonding states, respectively. More 4p-character of peak III can be ascribed to hybridization with Ti 4s and O 2p. Lower intensity of peak I in the case of cycled electrodes is also evidence of some reduction in Ti^{4+}. The XAS data provide additional confirmation of a hybrid redox mechanism for the composite materials; one in which both surface processes and intercalation contribute to the capacity.

CONCLUSIONS

In this work, we have demonstrated facile solution-based synthesis of lepidocrocite titanate – graphene composites by a self-assembly approach. The carbon content of Mg-coagulated LTO-rGO composites were tuned between 1 to 17%, whereas other coagulants (i.e., Li^+, Na^+, K^+) resulted in inhomogeneous mixtures of titania and reduced graphene oxide layers. The higher hydration of the Mg^{2+} cation, which results in a larger interlayer spacing, may account for the better homogeneity of the composites made this way. An increase in the interlayer spacing with carbon content was confirmed by XRD analysis and a correlation between interlayer spacing and the sum of carbon content and water was observed. As prepared LTO-rGO composite electrodes with at least 7% rGO without carbon additives display higher capacities than Mg-coagulated titania sheets with 10% acetylene black in sodium half-cell configurations. The redox mechanism appears to be a combination of diffusion-controlled and surface-limited processes as determined by power law analysis of cyclic voltammetry data on cells containing the LTO-14.5%rGO composite. Even at a low scan rate of 0.05 mV s^{-1} the mechanism is predominantly surface-limited (61%). This is substantially higher than that of a similar system of dopamine-derived LTO-30%C heterostructures (25%) at the same scan rate. A possible explanation is the presence of Mg^{2+} cations in the interlayer spaces of the LTO-rGO composites, which may impede diffusion of sodium cations. Another difference between the two systems was the dependence of capacity on carbon content. For the dopamine-derived samples, capacity scaled with carbon content, with the highest value observed for the sample containing 30% carbon (the highest value in the study). In contrast, the best results in the LTO-rGO system were obtained for the materials containing 8.5% and 14.5% carbon rather than the one with 17% rGO. These results indicate that the electrochemical properties of heterostructured materials is highly dependent upon details of synthesis, and the type of carbon used.

Supporting Information

Additional XRD patterns and SEM images of LTO-rGO composites, pictures of LTO-rGO suspensions and coagulated particles, EDS analysis of composites, galvanostatic electrochemical cycling, cyclic voltammogram and EIS data.

ACKNOWLEDGEMENTS

This work was supported as part of the Center for Mesoscale Transport Properties, an Energy Frontier Research Center supported by the U.S. Department of Energy, Office of Science, Basic Energy Sciences, under award #DE-SC0012673 including the following. Work at the Molecular Foundry of Lawrence Berkeley National Lab was supported by the Office of Science, Office of Basic Energy Sciences of the U.S. Department of Energy under Contract No. DE-AC02- 05CH11231. We would like to acknowledge the use of the Stanford Synchrotron Radiation Light source, SLAC National Accelerator Laboratory, that is supported by the U.S. Department of Energy, Office of Science, Office of Basic Energy Sciences under Contract No. DE-AC02-76SF00515. This document was prepared as an account of work sponsored by the United States Government. While this document is believed to contain correct information, neither the United States Government nor any agency thereof, nor the Regents of the University of California, nor any of their employees, makes any warranty, express or implied, or assumes any legal responsibility for the accuracy, completeness, or usefulness of any information, apparatus, product, or process disclosed, or represents that its use would not infringe privately owned rights. Reference herein to any specific commercial product, process, or service by its trade name, trademark, manufacturer, or otherwise, does not necessarily constitute or imply its endorsement, recommendation, or favoring by the United States Government or any agency thereof, or the Regents of the University of California. The views and

opinions of authors expressed herein do not necessarily state or reject those of the United States Government or any agency thereof or the Regents of the University of California. E. S. T. acknowledges the William and Jane Knapp Chair in Energy and the Environment.

REFERENCES

(1) Shirpour, M.; Cabana, J.; Doeff, M. New Materials Based on a Layered Sodium Titanate for Dual Electrochemical Na and Li Intercalation Systems. *Energy Environ. Sci.* **2013**, *6*, 2538.

(2) Doeff, M. M.; Cabana, J.; Shirpour, M. Titanate Anodes for Sodium Ion Batteries. *J. Inorg. Organomet. Polym. Mater.* **2014**, *24*, 5–14.

(3) Rudola, A.; Saravanan, K.; Mason, C. W.; Balaya, P. $Na_2Ti_3O_7$: An Intercalation Based Anode for Sodium-Ion Battery Applications. *J. Mater. Chem. A* **2013**, *1*, 2653.

(4) Katogi, A.; Kubota, K.; Chihara, K.; Miyamoto, K.; Hasegawa, T.; Komaba, S. Synthesis and Electrochemical Performance of C-Base-Centered Lepidocrocite-like Titanates for Na-Ion Batteries. *ACS Appl. Energy Mater.* **2018**, *1*, 3630–3635.

(5) Alvarado, J.; Barim, G.; Quilty, C. D.; Yi, E.; Takeuchi, K. J.; Takeuchi, E. S.; Marschilok, A. C.; Doeff, M. M. Optimization of Nonatitanate Electrodes for Sodium-Ion Batteries. *J. Mater. Chem. A* **2020**, *8*, 19917-19926.

(6) Shirpour, M.; Cabana, J.; Doeff, M. Lepidocrocite-Type Layered Titanate Structures: New Lithium and Sodium Ion Intercalation Anode Materials. *Chem. Mater.* **2014**, *26*, 2502–2512.

(7) Markus, I. M.; Engelke, S.; Shirpour, M.; Asta, M.; Doeff, M. Experimental and Computational Investigation of Lepidocrocite Anodes for Sodium-Ion Batteries. *Chem. Mater.* **2016**, *28*, 4284–4291.

(8) Yin, W.; Alvarado, J.; Barim, G.; Scott, M. C.; Peng, X.; Doeff, M. M. A Layered Nonstoichiometric Lepidocrocite-Type Sodium Titanate Anode Material for Sodium-Ion Batteries. *MRS Energy Sustain.* **2021**, *8*, 88-97.

(9) Gao, T.; Fjellvåg, H.; Norby, P. Protonic Titanate Derived from $Cs_xTi_{2-x/2}Mg_{x/2}O_4$ (x = 0.7) with Lepidocrocite-Type Layered Structure. *J Mater Chem* **2009**, *19*, 787–794.

(10) Reeves, K. G.; Ma, J.; Fukunishi, M.; Salanne, M.; Komaba, S.; Dambournet, D. Insights into Li^+, Na^+, and K^+ Intercalation in Lepidocrocite-Type Layered TiO_2 Structures. *ACS Appl. Energy Mater.* **2018**, *1*, 2078–2086.

(11) Xiong, P.; Ma, R.; Sakai, N.; Sasaki, T. Genuine Unilamellar Metal Oxide Nanosheets Confined in a Superlattice-like Structure for Superior Energy Storage. *ACS Nano* **2018**, *12*, 1768–1777.

(12) Xiong, P.; Wu, Y.; Liu, Y.; Ma, R.; Sasaki, T.; Wang, X.; Zhu, J. Two-Dimensional Organic–Inorganic Superlattice-like Heterostructures for Energy Storage Applications. *Energy Environ. Sci.* **2020**, *13*, 4834–4853.

(13) Deng, Y.; Wu, Z.; Liang, R.; Jiang, Y.; Luo, D.; Yu, A.; Chen, Z. Layer-Based Heterostructured Cathodes for Lithium-Ion and Sodium-Ion Batteries. *Adv. Funct. Mater.* **2019**, *29*, 1808522.

(14) Zhao, C.; Wang, X.; Kong, J.; Ang, J. M.; Lee, P. S.; Liu, Z.; Lu, X. Self-Assembly-Induced Alternately Stacked Single-Layer MoS_2 and N-Doped Graphene: A Novel van Der Waals Heterostructure for Lithium-Ion Batteries. *ACS Appl. Mater. Interfaces* **2016**, *8*, 2372–2379.

(15) Das, P.; Fu, Q.; Bao, X.; Wu, Z.-S. Recent Advances in the Preparation, Characterization, and Applications of Two-Dimensional Heterostructures for Energy Storage and Conversion. *J. Mater. Chem. A* **2018**, *6*, 21747–21784.

(16) Geim, A. K.; Grigorieva, I. V. Van Der Waals Heterostructures. *Nature* **2013**, *499*, 419–425.

(17) Xiong, P.; Zhang, F.; Zhang, X.; Wang, S.; Liu, H.; Sun, B.; Zhang, J.; Sun, Y.; Ma, R.; Bando, Y.; Zhou, C.; Liu, Z.; Sasaki, T.; Wang, G. Strain Engineering of Two-Dimensional Multilayered Heterostructures for beyond-Lithium-Based Rechargeable Batteries. *Nat. Commun.* **2020**, *11*, 3297.
(18) Zhu, Y.; Peng, W.; Li, Y.; Zhang, G.; Zhang, F.; Fan, X. Multiple Roles of a Heterointerface in Two-Dimensional van Der Waals Heterostructures: Insights into Energy-Related Applications. *J. Mater. Chem. A* **2019**, *7*, 23577–23603.
(19) Xiong, P.; Ma, R.; Sakai, N.; Nurdiwijayanto, L.; Sasaki, T. Unilamellar Metallic MoS_2 /Graphene Superlattice for Efficient Sodium Storage and Hydrogen Evolution. *ACS Energy Lett.* **2018**, *3*, 997–1005.
(20) Clites, M.; Andris, R.; Cullen, D. A.; More, K. L.; Pomerantseva, E. Improving Electronic Conductivity of Layered Oxides through the Formation of Two-Dimensional Heterointerface for Intercalation Batteries. *ACS Appl. Energy Mater.* **2020**, *3*, 3835–3844.
(21) Bärtsch, M.; Niederberger, M. The Role of Interfaces in Heterostructures. *ChemPlusChem* **2017**, *82*, 42–59.
(22) Wang, C.; Sakai, N.; Ebina, Y.; Kikuchi, T.; Snowdon, M. R.; Tang, D.; Ma, R.; Sasaki, T. Three-in-One Cathode Host Based on Nb_3O_8/Graphene Superlattice Heterostructures for High-Performance Li–S Batteries. *J. Mater. Chem. A* **2021**, *9*, 9952–9960.
(23) Xiong, P. et al., Two-Dimensional Unilamellar Cation-Deficient Metal Oxide Nanosheet Superlattices for High-Rate Sodium Ion Energy Storage. *ACS Nano* **2018**, *12*, 12337–12346.
(24) Barim, G.; Dhall, R.; Arca, E.; Kuykendall, T. R.; Yin, W.; Takeuchi, K. J.; Takeuchi, E. S.; Marschilok, A. C.; Doeff, M. M. Heterostructured Lepidocrocite Titanate-Carbon Nanosheets for Electrochemical Applications. *ACS Appl. Nano Mater.* **2022**, *5*, 678–690.
(25) Sasaki, T.; Kooli, F.; Iida, M.; Michiue, Y.; Takenouchi, S.; Yajima, Y.; Izumi, F.; Chakoumakos, B. C.; Watanabe, M. A Mixed Alkali Metal Titanate with the Lepidocrocite-like Layered Structure. Preparation, Crystal Structure, Protonic Form, and Acid−Base Intercalation Properties. *Chem. Mater.* **1998**, *10*, 4123–4128.
(26) Hou, J. et al., Macroscopic and Strong Ribbons of Functionality-Rich Metal Oxides from Highly Ordered Assembly of Unilamellar Sheets. *J. Am. Chem. Soc.* **2015**, *137*, 13200–13208.
(27) Li, D.; Müller, M. B.; Gilje, S.; Kaner, R. B.; Wallace, G. G. Processable Aqueous Dispersions of Graphene Nanosheets. *Nat. Nanotechnol.* **2008**, *3*, 101–105.
(28) Mähler, J.; Persson, I. A Study of the Hydration of the Alkali Metal Ions in Aqueous Solution. *Inorg. Chem.* **2012**, *51*, 425–438.
(29) Glendening, E. D.; Feller, D. Dication−Water Interactions: $M^{2+}(H_2O)_n$ Clusters for Alkaline Earth Metals M = Mg, Ca, Sr, Ba, and Ra. *J. Phys. Chem.* **1996**, *100*, 4790–4797.
(30) Tahir, M. N.; Oschmann, B.; Buchholz, D.; Dou, X.; Lieberwirth, I.; Panthöfer, M.; Tremel, W.; Zentel, R.; Passerini, S. Extraordinary Performance of Carbon-Coated Anatase TiO_2 as Sodium-Ion Anode. *Adv. Energy Mater.* **2016**, *6*, 1501489.
(31) Rudola, A.; Aurbach, D.; Balaya P. A New Phenomena in Sodium Batteries: Voltage Step Due to Solvent Interaction. *Electrochem. Commun.* **2014**, *46*, 56-59.
(32) Seh, Z. W.; Sun, J.; Sun, Y.; Cui Y. A Highly Reversible Room-Temperature Sodium Metal Anode. *ACS Central Science* **2015**, *1*, 449-455.
(33) Doi, K.; Yamada, Y.; Okoshi, M.; Ono, J.; Chou, C.-P.; Nakai, H.; Yamada, A. Reversible Sodium Metal Electrodes: Is Fluorine an Essential Interphasial Component? *Angew. Chem. Int. Ed.* **2019**, *58*, 8024-8028.

TOC Graphic

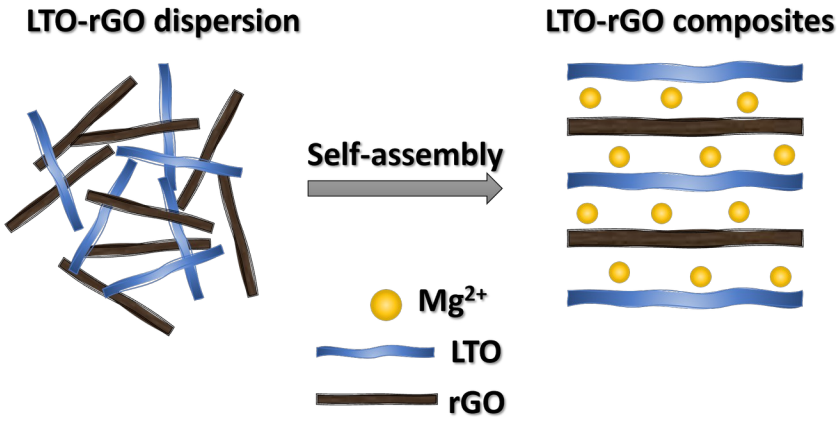
LTO-rGO dispersion
LTO-rGO composites
Self-assembly
Mg^{2+}
LTO
rGO